Arch. Metall. Mater. **63** (2018), 1, 467-472

DOI: 10.24425/118963

O. UZUN*, F. YILMAZ**#, C. EMEKSIZ***, S. ERGEN**, U. KOLEMEN**

CORRELATION OF HARDNESS AND SILICON MORPHOLOGY FOR Al-Si-Sb ALLOY

In this study, we have focused on the role of silicon morphology on the hardness of eutectic Al – 12 wt.% Si – 0.5 wt.% Sb alloy solidified at different cooling rates. The alloys were produced by using induction melting, arc-remelting and melt-spinning techniques. The cooling rates of the alloys were determined as 0.5, 60 and ~10^5°C.s^{-1} for induction-melted, arc-remelted and melt-spun alloy. The experimental results show that as the cooling rate increased the coarse silicon phase was substantially refined and its morphology altered from sharp need-like to round shape. Two exothermic peaks, attributed to precipitation and coarsening of silicon from supersaturated α-Al, were observed in the DSC curve of MS alloy. Vicker's hardness of melt-spun alloy was found two times higher than those of IMed and ARed alloys. The lowest hardness of induction-melted alloy was ascribed to the lamellar morphology of silicon, yielding decohesive rupture. This result was confirmed by finite element analyzing.

Keywords: Al-Si alloy; casting; Vickers; finite element analysis

1. Introduction

Over the last several decades, researchers have shown a growing interest to Al-Si alloys. Aluminum and silicon are the most abundant elements in the Earth's crust after oxygen. This fact leads to an increase in researches on Al and Si elements since the global demand for raw materials continues to increase, especially for iron. Al-Si alloys possess many unique properties, such as high wear resistance, moderate mechanical properties, excellent castability, machinability, low shrinkage, high corrosion resistance, high strength to weight ratio, which make these alloys suitable for engineering applications in automotive, aerospace and military industries [1-8]. The microstructure of the commercial eutectic Al-12Si alloy is composed of α-Al dendrites and eutectic silicon in the form of acicular and/or lamellar morphology [9]. The size, morphology and distribution of silicon phase in the matrix are the key to obtain an excellent product with desired mechanical properties [1,4]. The well adopted idea for improved mechanical properties in Al-Si alloys is the modification of Si morphology from course plate-like structure to a fine fibrous structure. [7,8]. Addition of certain impurity elements as a modifier, such as Na and Sr, or refiners, such as Al-Ti and Al-Ti-B, is one way to achieve fine and modified microstructure. [9-11]. Antimony is also effectively used for the refining of coarse Si plates [12]. Recently, Uzun et al. [2] have reported that as well as refining effect of Sb, the minor addition of Sb at high cooling rates can modify Si morphology into the fine fibrous structure.

Alternatively, a refined microstructure can be obtained by different casting techniques where the cooling rate is high. Induction melting (IM) and arc remelting (AR) are the most popular conventional techniques to produce commercial Al-Si alloys [3,11]. However, coarse plate-like eutectic Si and coarse columnar α-Al morphology usually exist in the microstructure of those alloys, which causes the poor mechanical properties [4]. This limitation of the conventional casting techniques led to the development of rapid solidification techniques such as gas atomization [13,14], spray casting [8], selective laser melting [6] and melt spinning, etc [5,15]. The rapid solidification techniques and conventional casting techniques differ from each other basically in terms of their cooling rate.

The refining effect of Sb in eutectic Al-Si alloys is well established in literature [2,16]. From the foregoing discussion, however, the different casting techniques are also of great importance to obtain desired alloy properties. So, there is still a lack of detailed studies on the effect of the casting techniques on the modification of Al-12Si-Sb alloy. In this research, Al-12Si-0.5Sb alloys were produced by induction-melting (IM), arc-remelting (AR) and melt-spinning (MS) techniques, and these techniques were compared in terms of their effects on the morphology and size of the eutectic Si and α-Al by using X-ray diffraction (XRD), optical microscopy (OM), scanning electron microscopy (SEM), differential scanning calorimeter (DSC) and transmission electron microscopy (TEM). Mechanical properties of the alloys were characterized by depth-sensing indentation technique. Distribution of maximum shear stress for different Si

* BULENT ECEVIT UNIVERSITY, DEPARTMENT OF METALLURGICAL AND MATERIAL SCIENCE ENGINEERING, ZONGULDAK, TURKEY
** GAZIOSMANPASA UNIVERSITY, DEPARTMENT OF PHYSICS, FACULTY OF ART AND SCIENCE, 60240, TOKAT, TURKEY
*** GAZIOSMANPASA UNIVERSITY, DEPARTMENT OF ELECTRICAL ENGINEERING, FACULTY OF NATURAL SCIENCES AND ENGINEERING, 60240, TOKAT, TURKEY
# Corresponding author: fikretyilmaz79@gmail.com

shapes was simulated using ANSYS 13.0 software to evaluate the relation between hardness and silicon morphology.

2. Experimental Details

The nominal composition of Al-12 wt.% Si-0.5 wt.% Sb were prepared from the high purity of Al (99.9% purity), Si (99.9% purity) and Sb (99.9% purity) elements. The first group of elements was weighed 20 g and then smelted trough induction furnace in a graphite crucible under argon atmosphere and slowly cooled to room temperature. The second group of elements were placed on water-cooled copper surface and melted by arc-remelting furnace under argon atmosphere. Received samples were cylindrical in shape with a diameter of 22 mm and a length of 6 mm. Each alloy was re-melted at least 5 times for improving the homogeneity of composition. Center sections of the specimens were used for metallographic examination. Melt-spun alloy was produced using a standard melt-spinner apparatus (Edmund Buhler, SC) under argon atmosphere, where the wheel speed is 40 ms^{-1}, ejection pressure is 200 mbar, and the wheel-nozzle distance is 0.2 mm. The resulting melt-spun alloy was typically ribbon in shape with the thickness of ~90 μm and wideness of 1 cm. The obtained alloys were named with respect to their production methods, such as IMed (Induction melted), ARed (Arc-remelted) and MS (melt-spun).

The cooling rate was directly measured using a thermocouple and it was determined as 0.5 and 60°C.s^{-1} for IMed and ARed alloys, respectively. For MS alloys, the cooling rate was calculated ~10^5°C.s^{-1} using an equation, $Q = (47/d)^3$, where d is the cell size in μm and Q is the cooling rate. The microstructures of the alloys were examined using optical microscopy (OM), scanning electron microscopy (SEM, LEO Evo40 VP) and transmission electron microscopy (TEM, Philips 420). The XRD measurements were carried out by Rigaku D/Max-IIIC diffractometer using CuKα radiation in 2θ range from 20° to 80°. Indentation experiments were conducted using dept-sensing indentation instrument of Shimadzu W201S with load and depth resolutions of ±19.6 μN and ±1 nm, respectively. Six different loads, from 200 to 1200 mN, were applied to each alloy at loading rate of 23.4 mNs^{-1}. Before indentation experiments, all alloys were polished using 4000 grit of SiC paper and diamond suspensions (3, 1 and 0.25 μm). Besides, the polished samples were etched with Keller's reagent for OM and SEM observation. The thermal analysis was performed using Seteram DSC-131 differential scanning calorimeter with the heating rate of 10 °C.min^{-1} under an argon flow in a temperature range of 100-450°C.

3. Results and Discussion

XRD patterns and corresponding main Al peak (111) of the alloys are illustrated in Fig. 1. All alloys exhibits the possible reflection peaks of Al and Si (Fig. 1a). The Si peaks are very shallow for MS alloy, suggesting that large amount of Si is dissolved in Al matrix to form the solid solution. This result indicates that the Si solubility in Al matrix has been extended by MS, which is in good agreement with previously reported study [17]. The solid solution can also be understood from Fig. 1b. According to the Bragg's law, the shifting of a diffraction peak to a lower angle refers an increasing in the inter-planar distance of main matrix. Here, Si atoms dissolved in Al-matrix (solid solution) bring about an extension in the inter-planar distance, manifesting a peak shift.

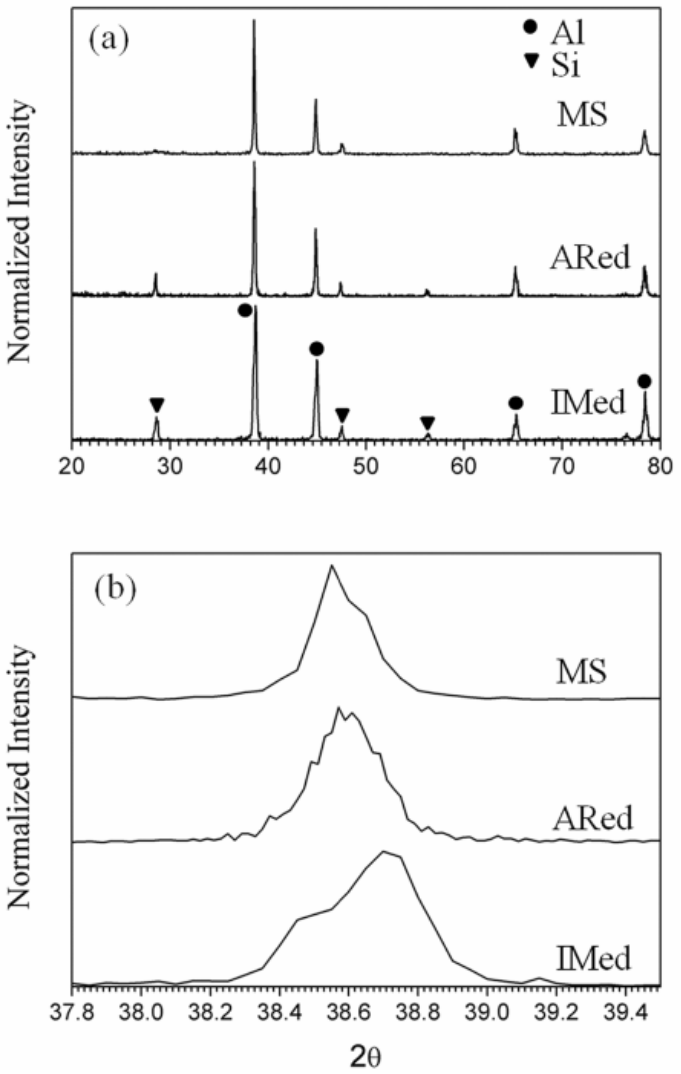

Fig. 1. (a) XRD diffraction patterns of the alloys and (b) the diffraction peak of (111) Al

Fig. 2a,c,e shows the OM micrographs of the alloys. The microstructures of the alloys consist of white and grey region, which represent Al and Si phase, respectively. IMed alloy exhibits typical eutectic lamellar structure, including needle-like Si, without any primary or plate-like Si (Fig. 2a). The particle size of Si needles ranges 10-20 μm. Although IMed alloy has the lowest cooling rate of 0.5°C, non-formation of plate like Si morphology reveals that Sb addition modify Si plates to some extent. The modification effect of Sb in Al-5.5Si alloy was pre-

viously reported by Fatahalla et al. [18]. The microstructure of ARed alloy consists of the mixture of two phases, fine eutectic Si and coarse columnar α-Al grains (Fig. 2c). In comparison to IMed alloy, the particle size of Si in ARed alloy is markedly refined, where the particle is nearly ~4 μm in size. The microstructure of MS alloy is composed of such a uniformly distributed fine eutectic mixture that it is difficult to distinguish from OM micrograph (Fig. 2e). The SEM micrographs showing eutectic Si morphology are depicted in Fig. 2b,d,f. The sharp-edge Si particles in IMed alloy turned into round-edge in ARed alloy, indicating the modification of Si grains because the cooling rate of arc-remelting technique is higher than that of induction melting (Fig. 2b,d). In the case of MS alloy, very fine branched dendrite structure is clearly seen (Fig. 2d). The MS alloy was also examined in detail by TEM (Fig. 3). TEM image clearly reveals that MS alloy shows typical hypoeutectic solidification structure which is composed of α-Al grains and eutectic grain boundaries. The grain boundaries as shown in Fig. 3 consist of homogeneously distributed nano-sized Si particles. Briefly, OP, SEM and TEM examinations reveal that the production techniques substantially affect the size and morphology of not only the eutectic Si but also α-Al grains. The degree of the refinement and modification mainly depends on solidification rate of production techniques. The solidification rate of AR technique is higher than that of IM since molten alloy is solidified on the water cooled copper surface. However, solidification rate in both techniques is notably low in comparison MS technique.

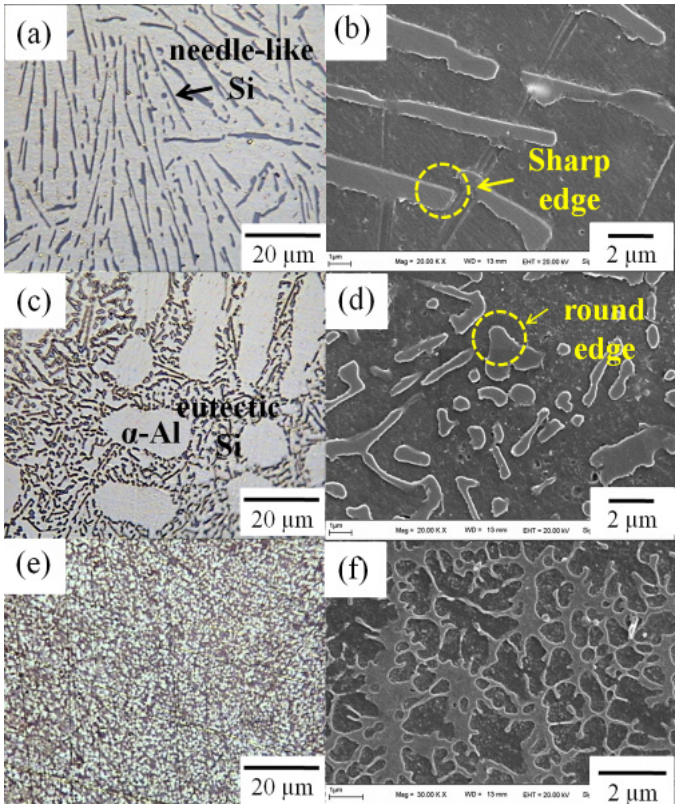

Fig. 2. Optic and SEM micrographs of the Al-12Si-0.5Sb alloy: (a) and (b) IMed, (c) and (d) ARed, (e) and (f) MS

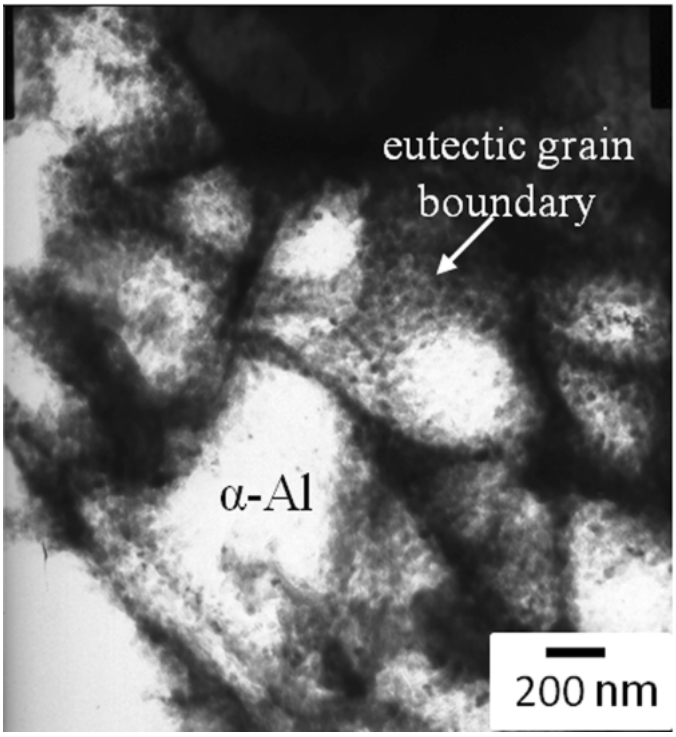

Fig. 3. TEM micrograph of the melt-spun alloy

Fig. 4 shows the DSC curves of the alloys in the temperature range of 100-450°C. There is no distinct peak for IMed but a very weak exothermic peak is seen for ARed alloy. In contrast, the alloy produced by MS shows two exothermic peaks around 234 and 346°C. The first exothermic peak was reported before and attributed to the precipitation of the Si from the supersaturated α-Al phase [19-21]. Since the exothermic peak in these alloys is proportional to the amount of Si precipitates, the degree of the super-saturation increases with increasing of the quenching rate. Second exothermic peak observed in MS alloy may be related to coarsening of Si precipitate. DSC and XRD results confirm that the Si solubility in Al-matrix extends with increasing cooling rate.

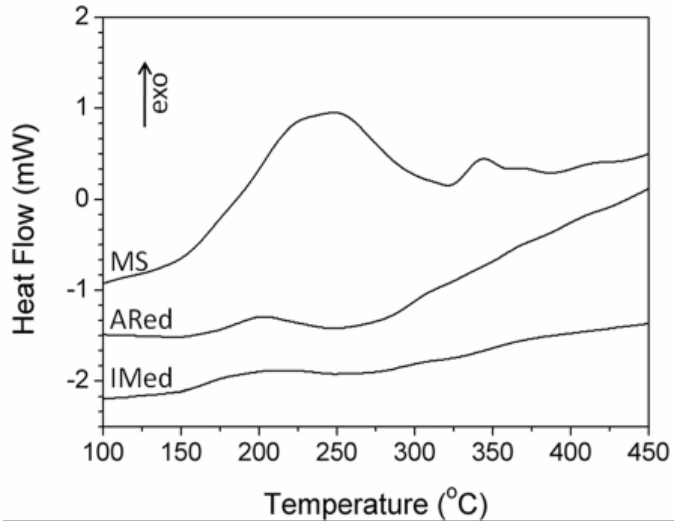

Fig. 4. DSC curves of the alloys obtained at the heating rate of 10°C/min.

Vickers hardness of the alloys at different indentation forces is depicted in Fig. 5. The deviation in hardness values of IMed and ARed alloys with increasing indentation forces is directly related to inhomogeneous microstructure of the alloys, which contains eutectic coarse Si particles. Unlike IMed and ARed alloys, the hardness of MS alloy non-linearly decreases with increasing indentation force and saturates at 800 mN. This behavior observed in hardness is called indentation size effect (ISE) and explained in terms of geometrically necessary dislocation (GND) approach [22]. The higher dislocation densities at shallow indentation depths intrinsically lead to higher hardness due to the Taylor relation [23]. Zong et al. [24] reported that the ISE is much more dominant in nano-scale regime (about <500 nm) than in micro-scale regime. They proposed that the hardness increases by a factor of about 2 at the indentation depths smaller than 500 nm. In our case, the indentation depths at the forces of 200, 400 and 600 mN are found as 2.1, 2.9 and 3.6 µm, which are much greater than nano-scale regime. Hence, GND is not account of ISE observed in MS alloy. On the other hand, it is well known that, in melt-spinning process, finer and more homogenous microstructure is expected in the wheel side of ribbons compared to its air side. Because the higher thermal conductivity of copper wheel in comparison to air leads to higher heat dissipation, namely higher cooling rate. For MS alloy, the indentation experiments were performed on the wheel side of ribbon. So, it is expected to higher hardness in the wheel side of ribbon at low forces for MS alloy. The indentation results given in Fig. 5 reveal that the hardness of MS alloy is about 2 times higher than that of other alloys, which can be clarified by two reasons: solid solution hardening and Hall-Petch hardening [25]. The size and shape of the Si particles is another important factor. The coarse lamellar Si particles existing in IMed alloy caused an apparent decrease in hardness. One can observe this situation from the indentation traces shown in Fig. 5. While the indentation traces of MS and ARed alloys are nearly uniform in shape, that of IMed alloy elongates perpendicular to direction of lamellar Si, resulting in much plastic deformation. In fact, much plastic deformation can be expected in lamellar structures since the cohesive strength of the different phases is mostly weak at the grain boundaries and this promotes decohesive rupture during indentation test. Fracture surface of the alloys are depicted in Fig. 6. The fracture in IMed alloy is predominantly intergranular with some transgranular contribution, which confirms decohesive rupture (Fig 6a). In literature, decohesive rupture is attributed to presence of the elements such as hydrogen, sulfur, phosphorus, antimony, arsenic at grain boundaries. Although the alloys in this work contain antimony, further investigation is needed to prove this argument. In addition, the broken Si-particles on the fracture surface of IMed suggest a typical brittle fracture. In the case of ARed alloy, the existing of dimples with broken

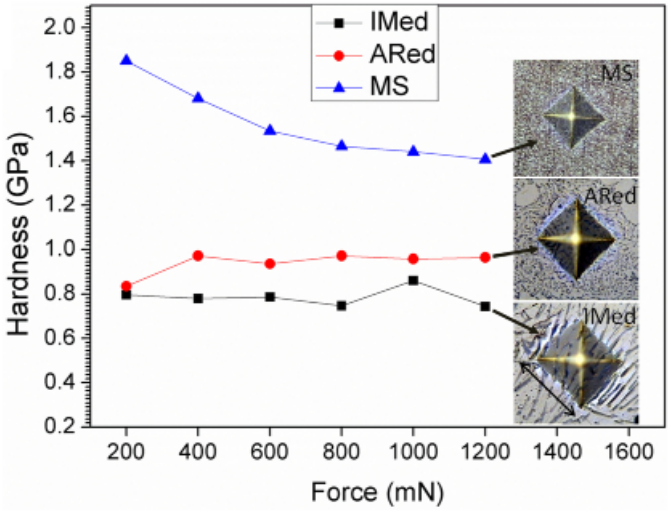

Fig. 5. Vickers microhardness of the alloys. The inset images show the indentation traces obtained at the force of 1200 mN

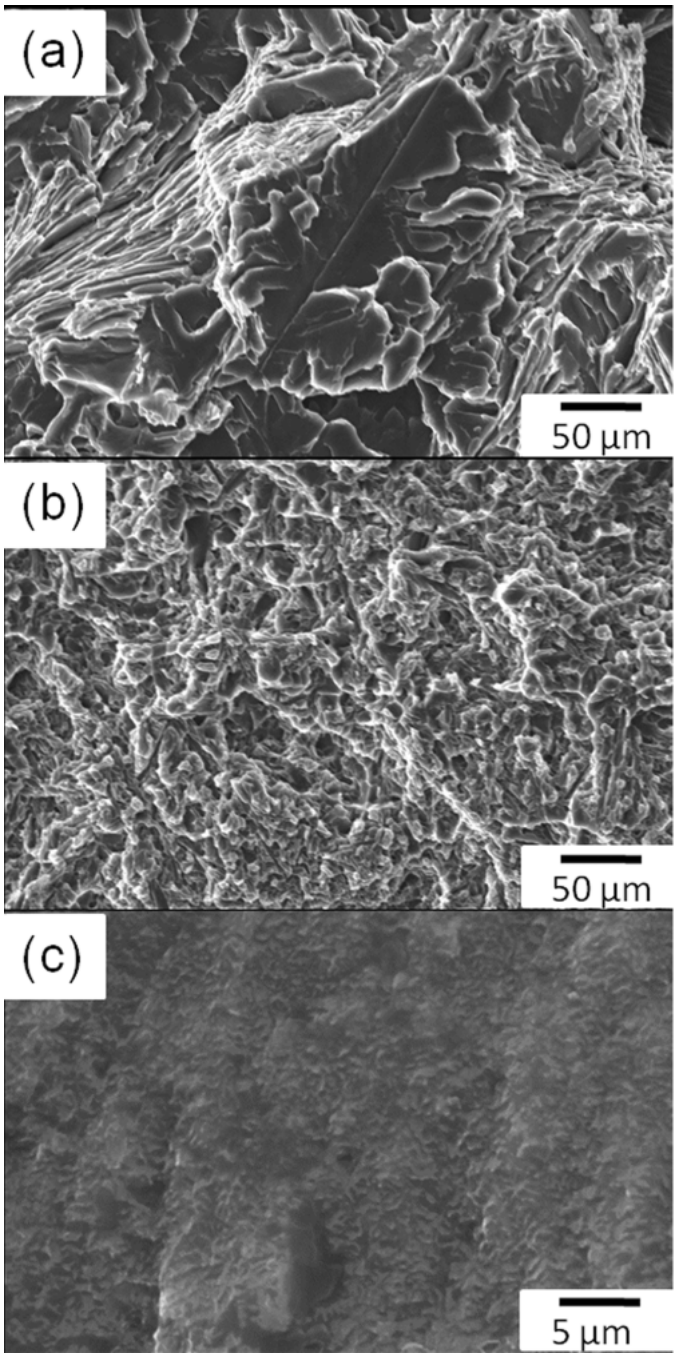

Fig. 6. SEM fractographs showing the fracture surface of (a) IMed, (b) ARed and (c) MS alloys

Si particles on the fracture surface indicates that the fracture in ARed alloy can be regarded as a mixing of brittle/ductile fracture (Fig. 6b). In MS alloy, the fracture surface is fully composed of typical dimple and ripple pattern, suggesting a ductile fracture. The fractographs demonstrate that modification and refinement of Si particles are the key factors to change the mechanism of fracture from brittle to ductile, which is in good agreement with observations reported earlier [25].

Finite element analysis was carried out to demonstrate the correlation between Si morphology and hardness. The maximum shear stress of lamellar type and equiaxed structures corresponding to the IMed and MS alloys are depicted in Fig. 7a and b, respectively. As shown in Fig. 7a, while maximum shear stress decreases in parallel to the lamellar structures (y-axis), it increases in the perpendicular direction (x-axis). On the other hand, as shown in Fig. 7b, the maximum shear stress is distributed nearly uniform in all direction. These results are in agreement with the hardness of alloys and confirmed the deformation of Al-Si substantially depends on Si morphology.

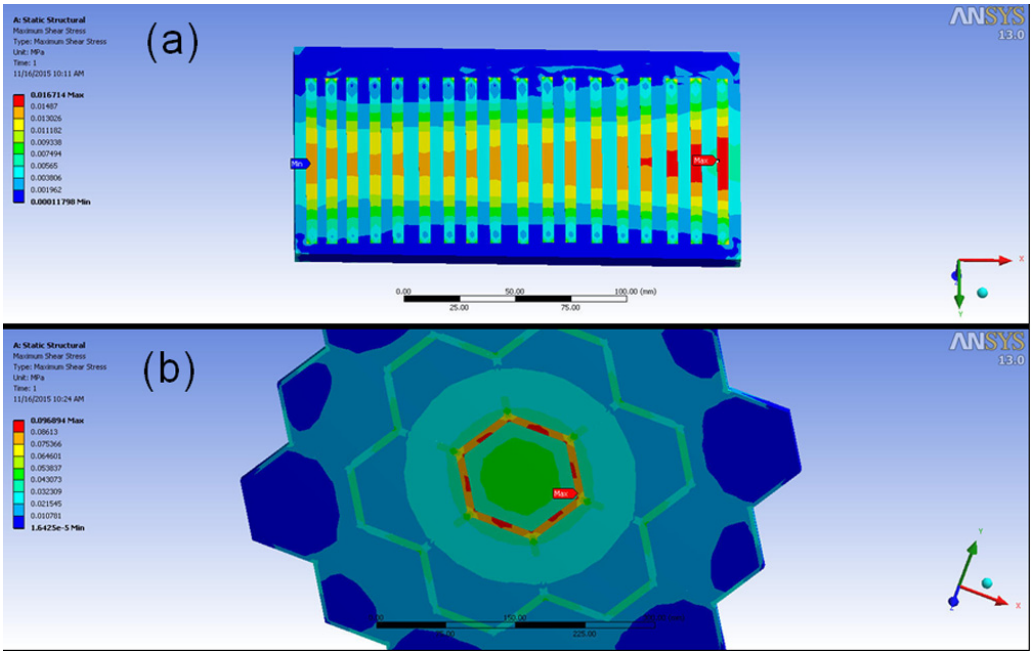

Fig. 7. Maximum shear stress results for (a) lamellar type structure and (b) equiaxed structure

4. Conclusions

In this research, eutectic Al-12Si-0.5Sb alloy were successfully obtained using induction melting (IM), arc-remelting (AR) and melt-spinning (MS) techniques. The results revealed that the production techniques have distinct effect on the microstructure and mechanical properties of the alloy. The main findings and conclusions can be summarized as follows:

– XRD results revealed that Si solubility in Al matrix were extended by MS technique. Two apparent exothermic peaks observed in DSC curve for MS alloy confirmed the extended solid solution, which were attributed to precipitation and coarsening of Si from supersaturated α-Al.
– IMed alloy exhibited typical eutectic lamellar structure with coarse needle-like Si. In ARed alloy, the coarse Si phase was refined to fine eutectic Si. Also, acicular Si phase was modified from sharp-edged to round-edge. The MS alloy showed hypoeutectic microstructure, consisting of cellular α-Al grains and eutectic grain boundaries. Nano-crystalline eutectic Si in grain boundaries were confirmed by TEM.
– Melt-spinning had a significant effect on increasing the hardness. Supersaturated solid solution and extremely fine microstructure were responsible of high hardness. Contrary to MS, IMed alloy exhibited the lowest hardness, which was attributed the lamellar structure. Observation of fracture surface of the alloys indicates that modification and refinement of Si particles are the key factors to alter the fracture mechanism from brittle to ductile mode.
– Finite element analysis confirmed that low hardness of IMed alloy depends on lamellar structure of Si.

Acknowledgements

This work was supported by Turkish State Planning Organization (DPT) (Project No: 2003K120510)

REFERENCES

[1] K.G. Basavakumar, P.G. Mukunda, M. Chakraborty, Mater. Design. **30**, 1258-1267 (2009).
[2] O. Uzun, F. Yilmaz, U. Kolemen, N. Basman, J. Alloy. Compd. **509,** 21-26 (2011).

[3] W. Zhang, Y. Liu, J. Yang, J. Dang, H. Xu, Z. Du, Mater. Charact. **66**, 104-110 (2012).
[4] J. Zhang, H. Yu, S.B. Kang, J.H. Cho, G. Min, V.Y. Stetsenko, J. Alloy. Compd. **541**, 157-162 (2012).
[5] M.F. Kilicaslan, F. Yilmaz, S. Ergen, S.J. Hong, O. Uzun, Mater. Charact. **77**, 15-22 (2013).
[6] X.J. Wang, L.C. Zhang, M.H. Fang, T.B. Sercombe, Mat. Sci. Eng. A-Struct. **597**, 370-375 (2014).
[7] C.G. Shivaprasad, S. Narendranath, V. Desai, S. Swami, M.S. Ganesha Prasad, Procedia Materials Science **5**, 1368-1375 (2014).
[8] K. Raju, S.H. Ojha, Procedia Materials Science **5**, 345-354 (2014).
[9] J.A. Lozano, B.S. Pena, Scripta. Mater. **54**, 943-947 (2006).
[10] L. Lu, K. Nogita, A.K. Dahle, Mat. Sci. Eng. A-Struct. **399**, 244-253 (2005).
[11] B.S. Pena, J.A. Lozano, Scripta. Mater. **54**, 1543-1548 (2006)
[12] A.K. Dahle, K. Nogita, S.D. McDonald, C. Dinnis, L. Lu, Mat. Sci. Eng. A-Struct. **413-414**, 243-248 (2005).
[13] L.H. Lee, H.J. Ko, T.S. Jeong, S.J. Hong, Curr. Nanoscience **10**, 146-150 (2014).
[14] M.F. Kilicaslan, J. Alloy. Compd. **606**, 86-91 (2014).
[15] M.F. Kilicaslan, F. Yilmaz, S.J. Hong, O. Uzun, Mat. Sci. Eng. A-Struct. **556**, 716-721 (2012).
[16] O. Uzun, T. Karaaslan, M. Keskin, J. Alloy. Compd. **358**, 104-111 (2003).
[17] M.L. Öveçoglu, M. Ünlü, N. Eruslu, A. Genç, Mater. Lett. **57**, 3296-3301 (2003).
[18] N. Fatahalla, M. Hafiz, M. Abdulkhalek, J. Mater. Sci. **34**, 3555-3564 (1999).
[19] N. Apaydın, R.W. Smith, Mater. Sci. Eng. **98**, 149-152 (1988).
[20] C. Antonione, L. Battezzati, F. Marino, J. Mater. Sci. Lett. **5**, 586-588 (1986).
[21] I. Yamauchi, K. Takahara, T. Tanaka, K. Matsubara, J. Alloy. Compd. **396**, 302-308 (2005).
[22] W.D. Nix, H. Gao, J. Mech. Phys. Solids **46** (3), 411-425 (1998).
[23] F.R.N. Nabarro (Ed.), J.P. Hirth (Ed.), Dislocations in solids **13**, 2007 Elsevier.
[24] Z. Zong, J. Lou, O.O. Adewoye, A.A. Elmustafa, F. Hammad, W.O. Soboyejo, Mat. Sci. Eng. A-Struct. **434**, 178-187 (2006).
[25] J.C.M. Li (Ed.), Microstructure and Properties of Materials **2**, 2000 World Scientific Publishing.